Inorganic Chemistry

Article

A New Hexanuclear Iron–Selenium Nitrosyl Cluster: Primary Exploration of the Preparation Methods, Structure, and Spectroscopic and Electrochemical Properties

Rongming Wang,*,†,‡ **Wei Xu,**† **Jian Zhang,**† **and Lijuan Li***,†

†*Department of Chemistry and Biochemistry, California State University, Long Beach, 1250 Bellflower Boulevard, Long Beach, California 90840, and* ‡*State Key Laboratory of Heavy Oil Processing, College of Chemistry & Chemical Engineering, China University of Petroleum, East China, Qingdao 266555, China*

A new hexanuclear iron–selenium nitrosyl cluster, $[(n\text{-Bu})_4N]_2[Fe_6Se_6(NO)_6]$ (**1**), and a hexanuclear iron–sulfur nitrosyl cluster, $[(n\text{-Bu})_4N]_2[Fe_6S_6(NO)_6]$ (**2**), were synthesized by the solvent-thermal reactions of $[(n\text{-Bu})_4N][Fe(CO)_3NO]$ with selenium or sulfur in methanol, while a tetranuclear iron–sulfur nitrosyl cluster, $(Me_4N)[Fe_4S_3(NO)_7]$ (**3**), was also prepared by the solvent-thermal reaction of $FeCl_2 \cdot 4H_2O$ with thiourea in the presence of $(CH_3)_4NCl$, $NaNO_2$, and methanol. Complexes **1**–**3** were characterized by IR, UV–vis, ^1H NMR, electrochemistry, and single-crystal X-ray diffraction analysis. IR spectra of complexes **1** and **2** show the characteristic NO stretching frequencies at 1694 and 1698 cm^{-1}, respectively, while the absorptions of complex **3** appear at 1799, 1744, and 1710 cm^{-1}. The UV–vis spectra of complexes **1**–**3** show different bands in the range of 259–562 nm, which are assigned to the transitions between orbitals delocalized over the Fe–S cluster, the ligand-to-metal charge transfer, π^*_{NO}–d_{Fe}, and the metal-to-ligand charge transfer, d_{Fe}–π^*_{NO}. Single-crystal X-ray structural analysis reveals that complex **1** crystallizes in the monoclinic $P2(1)/n$ space group with two molecules per unit cell. Two parallel "chair-shaped" structures, consisting of three iron and three selenium atoms, are connected by Fe–Se bonds with an average distance of 2.341 Å; each iron center is bonded to three selenium atoms and a nitrogen atom from the nitrosyl ligand with a pseudotetrahedral center geometry. Cyclic voltammograms of complexes **1** and **2** display two cathodic and three anodic current peaks with an unusually strong cathodic peak. Further electrochemical investigations demonstrated that the intensity of the unusually strong peak is a result of at least three processes. One is the quasi-reversible reduction, and the other two are from an irreversible electrochemical process, in which the compound goes through a typical electron transfer and chemical reaction mechanism. Compound **3** shows three quasi-reversible reductions.

Introduction

Several decades ago, scientists demonstrated that some iron–sulfur clusters were present at the active sites of a large number of enzymes and electron-transfer proteins; for instance, the cubane-like $[Fe_4S_4]$ cluster was found in ferredoxins and high-potential iron proteins,[1] and the sulfur-voided

$[Fe_4S_3]$ cuboidal subunit was found in the FeMo cofactor of nitrogenase.[2] Therefore, various iron–sulfur clusters including $[Fe_4S_4X_4]^{2-}$ (X = S-Me, S-Et, S-CH$_2$Ph, S-CH$_2$C$_6$H$_{11}$, Cl, Br),[3] $[Fe_6S_9(SR)]^{4-}$ (R = t-Bu, Ph),[4a] $[Fe_8S_6I_6]^{3-}$,[4b] $[Fe_6S_6X_6]^{2-}$ (X = Cl, Br, I),[4c,3b] $[Fe_6S_6(OC_6H_4\text{-}p\text{-}CH_3)_6]^{3-}$,[4d] $[Fe_4S_3MS_3(PEt_3)\text{-}Cl]$ (M = V, Mo),[4e] and $[Fe_3S_4(LS_3)]^{3-}$ [LS$_3$ = 1,3,5-tris[(4,6-dimethyl-3-mercaptophenyl)thio]-2,4,6-tris(p-tolylthio)benzene-(3−)][4f,3c] were synthesized to simulate these active sites. Because the only structurally authenticated example of $[Fe_4S_3]$ was foremost found in Roussin's black salt anion $[Fe_4S_3(NO)_7]^-$, several iron–sulfur nitrosyl clusters, such as $[Fe_4S_3(NO)_7]^{1-,2-,3-}$,[5]

*To whom correspondence should be addressed. E-mail: lli@csulb.edu (L.L.), qwrm@yahoo.com.cn (R.W.).

(1) (a) Stephan, D. W.; Papaefthymiou, G. C.; Frankel, R. B.; Holm, R. H. *Inorg. Chem.* **1983**, *22*, 1550–1557. (b) Johnson, R. E.; Papaefthymiou, G. C.; Frankel, R. B.; Holm, R. H. *J. Am. Chem. Soc.* **1983**, *105*, 7280–7287. (c) Daku, L. M. L.; Pécaut, J.; Lenormand-Foucaut, A.; Vieux-Melchior, B.; Iveson, P.; Jordanov, J. *Inorg. Chem.* **2003**, *42*, 6824–6850.

(2) (a) Christou, G.; Mascharak, P. K.; Armstrong, W. H.; Papaefthymiou, G. C.; Frankel, R. B.; Holm, R. H. *J. Am. Chem. Soc.* **1982**, *104*, 2820–2831. (b) Armstrong, W. H.; Mascharak, P. K.; Holm, R. H. *J. Am. Chem. Soc.* **1982**, *104*, 4373–4383. (c) Zuo, J. L.; Zhou, H. C.; Holm, R. H. *Inorg. Chem.* **2003**, *42*, 4624–4631.

(3) (a) Averill, B. A.; Herskovitz, T.; Holm, R. H.; Ibers, J. A. *J. Am. Chem. Soc.* **1973**, *95*, 3523–3534. (b) Coucouvanis, D.; Kanatzidis, M. G.; Dunham, W. R.; Hagen, W. R. *J. Am. Chem. Soc.* **1984**, *106*, 7998–7999. (c) Rao, P. V.; Holm, R. H. *Chem. Rev.* **2004**, *104*, 527–559.

(4) (a) Christou, G.; Holm, R. H.; Sabat, M.; Ibers, J. A. *J. Am. Chem. Soc.* **1981**, *103*, 6269–6271. (b) Pohl, S.; Saak, W. *Angew. Chem., Int. Ed. Engl.* **1984**, *23*, 907–908. (c) Saak, W.; Henkel, G.; Pohl, S. *Angew. Chem., Int. Ed. Engl.* **1984**, *23*, 150–151. (d) Kanatzidis, M. G.; Salifoglou, A.; Coucouvanis, D. *J. Am. Chem. Soc.* **1985**, *107*, 3358–3360. (e) Cen, W.; MacDonnell, F. M.; Scott, M. J.; Holm, R. H. *Inorg. Chem.* **1994**, *33*, 5809–5818. (f) Zhou, J.; Holm, R. H. *J. Am. Chem. Soc.* **1995**, *117*, 11353–11354.

(5) (a) Johansson, G.; Lipscomb, W. N. *Acta Crystallogr.* **1958**, *11*, 594–598. (b) Chu, C. T.-W.; Dahl, L. F. *Inorg. Chem.* **1977**, *16*, 3245–3251. (c) D'Addario, S.; Demartin, F.; Grossi, L.; Iapalucci, M. C.; Laschi, F.; Longoni, G.; Zanello, P. *Inorg. Chem.* **1993**, *32*, 1153–1160.

$[Fe_4S_4(NO)_4]^{0,1-}$,[6] and $[Fe_6S_6(NO)_6]^{2-}$,[7] were also obtained. Recently, because the important functions of nitric oxide (NO) in diverse physiological processes have been gradually recognized by researchers,[8,9] some of which include controlling the blood pressure, regulating gene transcription, inhibiting tumor growth, modulating vasodilation, smoothing muscle proliferation, and acting as biological messengers, these iron–sulfur nitrosyl clusters caught people's attention once more as potential physiological NO donors.[10] However, some clusters, such as $[Fe_6S_6(NO)_6]^{2-}$, were obtained only by complicated multistep procedures.[7a] Subsequently, a new $[Fe_8S_6(NO)_8]^{2-}$ cluster was synthesized with an improved one-step synthetic method, in which $[Fe_4S_3(NO)_7]^-$ was used as one of the starting materials.[11] Yet, despite many known examples of iron–sulfur nitrosyl clusters, iron–selenium nitrosyl clusters are extremely rare. To date, only one iron–selenium nitrosyl cluster, $(Ph_4As)[Fe_4Se_3(NO)_7]$, has been reported, with no characterization other than its structure.[12] Interestingly, Surerus and co-workers[13] demonstrated through Mössbauer and electron paramagnetic resonance (EPR) spectra that the cluster binding site of beef heart aconitase can bind not only to iron–sulfur clusters, including $[Fe_4S_4]^{2+,1+}$ (in the active enzyme), the cubane $[Fe_3S_4]^{1+,0}$, and the linear $[Fe_3S_4]^+$, but also to iron–selenium clusters, including $[Fe_4Se_4]^{2+}$ and $[Fe_3S_4]^{1+,0}$. In addition, the selenium analogue $[Fe_4Se_4]$ aconitase was found to have higher catalytic activity than the native sulfur-containing enzyme when isocitrate was used as the substrate.

Our work focuses on the synthesis of iron nitrosyl compounds containing a polynuclear framework, and we have reported a cyclic tetranuclear cluster, $[Fe(NO)_2(imidazolate)]_4$, and several dinuclear iron compounds, $[Fe_2(\mu\text{-RS})_2(NO)_4]$ (R = *n*-Pr, *t*-Bu, 6-methyl-2-pyridyl, and 4,6-dimethyl-2-pyrimidyl).[14] Here we report the syntheses, characterizations, and structures of a new hexanuclear iron–selenium nitrosyl cluster, $[(n\text{-Bu})_4N]_2[Fe_6Se_6(NO)_6]$ (**1**), a hexanuclear iron–sulfur nitrosyl cluster, $[(n\text{-Bu})_4N]_2[Fe_6S_6(NO)_6]$ (**2**), and a tetranuclear iron–sulfur nitrosyl cluster, $(Me_4N)[Fe_4S_3(NO)_7]$ (**3**). The syntheses and investigations of these complexes help us gain insight on the structures of iron nitrosyl clusters and establish the important relationship between the structures and functions of these molecules.

Experimental Section

Materials and Methods. $[(n\text{-Bu})_4N][Fe(CO)_3NO]$ was synthesized according to the reported procedure but with substitution of $(n\text{-Bu})_4NCl$ for $(n\text{-Bu})_4NBr$.[15] Other chemicals were purchased from Aldrich Chemical Co. and were used without further purification. All solvents were purified and/or dried by standard techniques and degassed under vacuum prior to use, and all experiments were conducted under a nitrogen atmosphere without a special description. IR spectra were recorded on a Nicolet AVATAR 370 FTIR spectrophotometer. UV–vis spectra were measured on a Varian Cary 300 Bio UV–vis spectrophotometer. The ^1H NMR spectra were obtained on a Bruker 400 MHz NMR spectrometer, using acetonitrile-d_3 as the solvent and tetramethylsilane as the internal standard.

Synthesis of $[(n\text{-Bu})_4N]_2[Fe_6Se_6(NO)_6]$ (1). $[(n\text{-Bu})_4N][Fe(CO)_3NO]$ (103 mg, 0.25 mmol), selenium (79 mg, 1 mmol), and methanol (4 mL) were mixed in a vial under a nitrogen atmosphere. The vessel was then sealed and heated at 85 °C for 48 h. The autoclave was subsequently allowed to cool to room temperature. After the reaction solution was filtered and washed using methanol, a black solid was obtained. The black solid was then dissolved in acetonitrile, and diethyl ether was slowly added to the solution. The mixed solution was placed in a glovebox at −35 °C overnight to crystallize. The black crystals, suitable for X-ray crystallography, were collected by filtration, washed with methanol, and dried under vacuum for several hours. Yield: 52 mg (85%, based on $[(n\text{-Bu})_4N][Fe(CO)_3NO]$). FTIR: ν_{NO} 1694 (CH_3CN), 1683 (KBr) cm^{-1}. UV–vis spectrum: 259, 297 nm (CH_3CN). ^1H NMR $(CD_3CN$, ppm): 3.06 (t, 8H), 1.58 (m, 8H), 1.32 (m, 8H), 0.95 (t, 12H).

Synthesis of $[(n\text{-Bu})_4N]_2[Fe_6S_6(NO)_6]$ (2). Compound **2** was obtained using sulfur (32 mg, 1 mmol) by the same procedure at 120 °C as that described above for **1**. Yield: 46 mg (92%, based on $[(n\text{-Bu})_4N][Fe(CO)_3NO]$). FTIR: ν_{NO} 1698 (CH_3CN), 1678 (KBr) cm^{-1}. UV–vis spectrum: 288 nm (CH_3CN). ^1H NMR $(CD_3CN$, ppm): 3.06 (t, 8H), 1.58 (m, 8H), 1.33 (m, 8H), 0.95 (t, 12H).

Synthesis of $(Me_4N)[Fe_4S_3(NO)_7]$ (3). $FeCl_2 \cdot 4H_2O$ (97.3 mg), thiourea (116.2 mg), $(CH_3)_4NCl$ (57.5 mg), $NaNO_2$ (108.8 mg), and methanol (3 mL) were mixed in a vial under a nitrogen atmosphere. The vessel was sealed and heated at 85 °C for 48 h. The autoclave was then allowed to cool to room temperature. The solution was filtered and washed using methanol, and the solid mixture was dissolved in acetonitrile and filtered to remove the undissolved white solid. Subsequently, diethyl ether was slowly added to the solution, and the mixed solution was placed in a glovebox at −35 °C overnight to crystallize. The black crystals, suitable for X-ray crystallography, were collected by filtration, washed with methanol, and dried under vacuum for several hours. Yield: 33 mg (88%, based on $FeCl_2 \cdot 4H_2O$). FTIR: ν_{NO} 1799, 1744, 1710 (CH_3CN), 1798, 1728, 1712 (KBr) cm^{-1}. UV–vis spectrum: 265, 357, 434, 584 nm (CH_3CN). ^1H NMR $(CD_3CN$, ppm): 3.05 (s, 12H).

X-ray Crystallography. Complexes **1**–**3** were glued to a thin glass fiber with epoxy resin and collected on a Bruker APEX II diffractometer equipped with a fine-focus, 2.0-kW sealed-tube X-ray source (Mo Kα radiation, $\lambda = 0.7103$ Å) operating at 50 kV and 30 mA at 273 K. The crystallographic collection and refinement parameters for complexes **1** and **3** are listed in Table 1.

(6) (a) Gall, R. S.; Chu, C. T.-W.; Dahl, L. F. *J. Am. Chem. Soc.* **1974**, *96*, 4019–4023. (b) Chu, C. T.-W.; Lo, F. Y.-K.; Dahl, L. F. *J. Am. Chem. Soc.* **1982**, *104*, 3409–3422.

(7) (a) Scott, M. J.; Holm, R. H. *Angew. Chem., Int. Ed. Engl.* **1993**, *32*, 564–566. (b) Geiser, U.; Williams, J. M. *Acta Crystallogr.* **1998**, *C54*, 292–293.

(8) (a) Culotta, E.; Koshland, D. E. *Science* **1992**, *258*, 1862–1865. (b) Maes, E. M.; Walker, F. A.; Montfort, W. R.; Czernuszewicz, R. S. *J. Am. Chem. Soc.* **2001**, *123*, 11664–11672. (c) Dall'Agnol1, M.; Bernstein1, C.; Bernstein1, H.; Garewal1, H.; Payne1, C. M. *Proteomics* **2006**, *6*, 1654–1662.

(9) (a) Bredt, D. S.; Hwang, P. M.; Glatt, C. E.; Lowenstein, C.; Reed, R. R.; Snyder, S. H. *Nature* **1991**, *351*, 714–718. (b) Abu-Soud, H.; Stuehr, D. J. *Proc. Natl. Acad. Sci. U.S.A.* **1993**, *90*, 10769–10772. (c) Griffith, O. W.; Stuehr, D. J. *Annu. Rev. Physiol.* **1995**, *57*, 707–736. (d) Heo, J.; Campbell, S. L. *Biochemistry* **2004**, *43*, 2314–2322.

(10) (a) Bourassa, J.; DeGraff, W.; Kudo, S.; Wink, D. A.; Mitchell, J. B.; Ford, P. C. *J. Am. Chem. Soc.* **1997**, *119*, 2853–2860. (b) Ford, P. C.; Bourassa, J.; Miranda, K.; Lee, B.; Lorkovic, I.; Boggs, S.; Kudo, S.; Laverman, L. *Coord. Chem. Rev.* **1998**, *117*, 185–202. (c) De Leo, M.; Ford, P. C. *J. Am. Chem. Soc.* **1999**, *121*, 1980–1981. (d) Works, C. F.; Ford, P. C. *J. Am. Chem. Soc.* **2000**, *122*, 7592–7593. (e) Bourassa, J. L.; Ford, P. C. *Coord. Chem. Rev.* **2000**, *200–202*, 887–900. (f) Wecksler, S.; Mikhailoysky, A.; Ford, P. C. *J. Am. Chem. Soc.* **2004**, *126*, 13566–13567.

(11) Kalyvas, H.; Coucouvanis, D. *Inorg. Chem.* **2006**, *45*, 8462–8564.

(12) (a) Barnes, J. C.; Glidewell, C.; Lees, A.; Howie, R. A. *Acta Crystallogr.* **1990**, *C46*, 2051–2053. (b) Chen, T.-N.; Lo, F.-C.; Tsai, M.-L.; Shih, K.-N.; Chiang, M.-H.; Lee, G.-H.; Liaw, W.-F. *Inorg. Chim. Acta* **2006**, *359*, 2525–2533.

(13) (a) Surerus, K. K.; Kennedy, M. C.; Beinert, H.; Münck, E. *Proc. Natl. Acad. Sci. U.S.A.* **1989**, *86*, 9846–9850. (b) Beinert, H.; Kennedy, M. C. *Eur. J. Biochem.* **1989**, *186*, 5–15.

(14) (a) Wang, X.; Sundberg, E. B.; Li, L.; Kantardjieff, K. A.; Herron, S. R.; Lim, M.; Ford, P. C. *Chem. Commun.* **2005**, 477–479. (b) Wang, R.; Camacho-Fernandez, M. A.; Xu, W.; Zhang, J.; Li, L. *Dalton Trans.* **2009**, 777–786.

(15) Xu, Y. Y.; Zhou, B. *J. Org. Chem.* **1987**, *52*, 974–977.

Table 1. Crystallographic Collection and Refinement Parameters for **1** and **3**

	1	**3**
formula	$C_{32} H_{72} N_8 O_6 Se_6 Fe_6$	$C_4 H_{12} N_8 O_7 S_3 Fe_4$
M_r	1473.84	603.80
size [mm^3]	$0.18 \times 0.14 \times 0.10$	$0.14 \times 0.12 \times 0.08$
cryst syst	monoclinic	triclinic
space group	$P2(1)/n$	$P\bar{1}$
a [Å]	12.0207(6)	8.8970(9)
b [Å]	11.8711(6)	9.5905(10)
c [Å]	18.5002(12)	11.7278(12)
α [deg]	90	86.1650(10)
β [deg]	95.416(4)	74.0230(10)
γ [deg]	90	88.3620(10)
V [Å^3]	2628.2(3)	959.83(17)
Z	2	2
$F(000)$	1456	600
ρ_{calcd} [g cm^{-3}]	1.862	2.089
θ [mm^{-1}]	5.811	3.333
range [deg]	1.94−25.14	2.71−24.83
reflns collcd	4575	3238
indep reflns	3463 (R_{int} = 0.0317)	2883 (R_{int} = 0.0388)
parameters	271	235
R1 [$I > 2\sigma(I)$]	0.0527	0.0419
wR2 [$I > 2\sigma(I)$]	0.0779	0.0973
GOF	0.995	1.025

The structure of complex **2** was omitted because it resembles the one reported.[7b] The empirical absorption correction was based on equivalent reflections, and other possible effects such as absorption by the glass fiber were simultaneously corrected. Each structure was solved by direct methods followed by successive difference Fourier methods. All non-hydrogen atoms were refined anisotropically. Computations were performed using *SHELXTL*, and final full-matrix refinements were against F^2. The *SMART* software was used for collecting frames of data, indexing reflections, and determining lattice constants, *SAINT-PLUS* for integration of the intensity of the reflections and scaling, *SADABS* for absorption correction, and *SHELXTL* for space groups and structure determinations, refinements, graphics, and structure reporting.[16−18]

Electrochemistry. Cyclic voltammetry (CV) was carried out with a CH Instruments 730A electrochemical analyzer. A three-electrode system consisting of a platinum working electrode, a platinum wire counter electrode, and an Ag/Ag$^+$ reference electrode was used. The reference electrode was separated from the bulk solution by a fritted-glass bridge filled with the solvent/supporting electrolyte mixture. The CV data were recorded with a scan rate ranging from 100 mV s^{-1} to 1 V s^{-1}. All potential values are reported versus the ferrocene/ferrocenium ion, and $E_{1/2}°[Fe(Cp)_2/Fe(Cp)_2^+]$ under our experimental conditions is 0.08 V for all complexes **1−3**.

Results and Discussion

Synthesis of the Complexes. It has been demonstrated that iron−sulfur nitrosyl clusters can be synthesized by the reactions of ferrous compounds, nitrosyl donor compounds, and sulfur donor reagents at room temperature or under heating conditions.[5−7,11,19] In order to prepare and isolate new classes of iron−sulfur (selenium) nitrosyl clusters and to investigate their properties, solvent-thermal

reactions at high pressure were carried out under a nitrogen atmosphere and monitored by FTIR spectroscopy. Complex **1** was prepared by the reaction of 1 equiv of [(n-Bu)$_4$-N][Fe(CO)$_3$NO][15] and 4 equiv of selenium in methanol. Upon reaction, the characteristic IR absorptions of the nitroysl group (ν_{NO}) were shifted to lower frequencies as the carbonyls were substituted by selenium. Meanwhile, the orange reaction solution gradually turned to dark black. The observations are consistent with the results obtained from NMR and single-crystal X-ray diffraction. Complex **1** was obtained as a black solid with 85% yield. In order to prove the generality of this new synthetic method, a hexanuclear iron−sulfur nitrosyl cluster, **2**, was synthesized using similar solvent-thermal reactions with sulfur donor reagents in high yield of 92%, and a tetranuclear cluster, **3**, was also prepared by the solvent-thermal reaction of FeCl$_2$·4H$_2$O, thiourea, (CH$_3$)$_4$NCl, and NaNO$_2$ in methanol with 88% yield. Complexes **1−3** are all fairly stable in the solid state and in solution under air. Single crystals of complexes **1−3** suitable for X-ray diffraction analysis were obtained by the slow diffusion of diethyl ether into an acetonitrile solution at −35 °C. Complexes **1** and **2** are soluble in most polar organic solvents including acetonitrile, dichloromethane, and tetrahydrofuran but are insoluble in methanol, ethyl ether, and hexane, while complex **3** is more or less soluble in all organic solvents. The results show that the solvent-thermal reaction is a more effective and simpler procedure for the synthesis of polynuclear iron nitrosyl compounds than the reported methods, in which other iron−sulfur nitrosyl clusters, [Fe$_4$S$_4$(NO)$_4$] for (Et$_4$N)$_2$-[Fe$_6$S$_6$(NO)$_6$][7a] and (NH$_4$)[Fe$_4$S$_3$(NO)$_7$] for (PPN)$_2$[Fe$_8$S$_6$-(NO)$_8$],[11] were used as starting materials. Although (PPN)-[Fe$_4$Se$_3$(NO)$_7$] could be prepared from (PPN)[Fe(CO)$_3$NO], it was via an intermediate (PPN)[Se$_5$Fe(NO)$_2$] and in a low yield of 21%.[12b]

Spectroscopic Characterization. The FTIR spectrum of **1** in acetonitrile shows a NO stretching frequency at 1694 cm^{-1}, which is located in the range corresponding to NO$^+$.[20] The value is similar to the corresponding absorptions at 1698 cm^{-1} for **2** and is situated in the range of the absorptions at 1748, 1689, and 1660 cm^{-1} for [Fe$_4$S$_3$-(NO)$_7$]$^{2-}$[5c] but lower than the values 1799, 1744, and 1710 cm^{-1} for **3**. These observations indicate that there are significantly more back-donations from the metal to the π^* orbital of the nitrosyls for complexes **1**, **2**, and [Fe$_4$S$_3$(NO)$_7$]$^{2-}$ than for complex **3** because the latter is a monoanion. This is consistent with the results of single-crystal X-ray diffraction analysis, which revealed that nitrosyl moieties of the four complexes are all near-linear, but the bond distances N−O for **1**, **2**, and [Fe$_4$S$_3$(NO)$_7$]$^{2-}$ are longer than that of **3**.

The electronic absorption spectra of complexes **1−3** were measured in acetonitrile. As shown in Figure 1, complex **1** shows a medium band at 288 nm and a weak band at 554 nm. The absorptions mainly arise from the transitions between orbitals delocalized over the Fe−Se cluster, the ligand-to-metal charge transfer (LMCT), $\pi^*_{NO}-d_{Fe}$, and the metal-to-ligand charge transfer (MLCT), $d_{Fe}-\pi^*_{NO}$. The bands over 400 nm are ascribed to the LMCT, while the bands at higher energy are

(16) *SMART and SAINT for Windows NT Software Reference Manuals*, version 5.0; Bruker Analytical X-ray Systems: Madison, WI, 1997.

(17) Sheldrick, G. M. *SADABS—A Software for Empirical Absorption Correction*; University of Göttingen: Göttingen, Germany, **1997**.

(18) *SHELXTL Reference Manual*, version 5.1; Bruker Analytical X-ray System: Madison, WI, 1997.

(19) Hsu, I.-J.; Hsieh, C.-H.; Ke, S.-C.; Chiang, K.-A.; Lee, J.-M.; Chen, J.-M.; Jang, L.-Y.; Lee, G.-H.; Wang, Y.; Liaw, W.-F. *J. Am. Chem. Soc.* **2007**, *129*, 1151–1159.

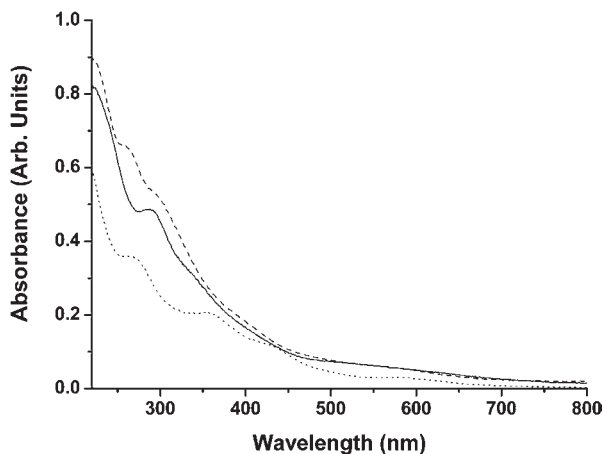(20) Wang, P. G.; Cai, T. B.; Taniguchi, N. *Nitric Oxide Donors*; Wiley-VCH: New York, 2005.

Figure 1. Electronic absorption spectra of complexes **1** (solid line), **2** (dashed line), and **3** (dotted line) in acetonitrile.

thought to be from MLCT and the transitions within the Fe−Se cluster.[21] Similarly, complex **2** shows two medium bands at 259 and 297 nm and a weak band at 552 nm, whereas complex **3** displays four bands at 265, 357, 425, and 562 nm.

Structural Studies. The molecular structures of complexes **1**−**3** were determined by X-ray diffraction analysis, and it was found that the structural parameters of complex **2** resembled the one reported.[7b] The selected bond lengths and bond angles are listed in Table 2. The crystal structure of **1** is monoclinic and crystallized in a $P2(1)/n$ space group with two molecules per unit cell. As shown in Figure 2, two parallel "chair-shaped" structures, consisting of three iron and three selenium atoms, are connected by Fe−Se bonds with an average distance of 2.341 Å, and each iron center is bonded to three selenium atoms and a nitrogen atom from the nitrosyl ligand with a pseudo-tetrahedral center geometry. The $[Fe_6S_6(NO)_6]^{2-}$ cluster had been prepared previously with different counterions but in a more complicated procedure.[7,11] For the crystal structure of **3**, no differences could be attributed to effects of the counterion besides the packing effects, which is related with the distortions of the Fe_4S_3 core.[5c]

The average Fe−Fe distance of 2.730 Å for **1** suggests that there is fairly strong interaction between the two iron centers. It is longer than the relevant value of 2.644 Å for **2** because the radius of the selenium atom is larger than that of sulfur. This is in agreement with the average value of 2.341 Å for the Fe−Se interactions in the $[Fe_6Se_6(NO)_6]^{2-}$ cluster and 2.220 Å for the Fe−S interactions in the $[Fe_6S_6(NO)_6]^{2-}$ cluster. Interestingly, the average Fe−Fe distance of 2.644 Å for $[Fe_6S_6(NO)_6]^{2-}$, even 2.730 Å for $[Fe_6Se_6(NO)_6]^{2-}$ or 2.705 Å for **3**, is clearly shorter than the relevant value of 2.764 Å for dianion $[Fe_4S_3-(NO)_7]^{2-}$.[5c] This difference can be explained by the following. On the one hand, the $[Fe_6S_6(NO)_6]^{2-}$ and $[Fe_6Se_6(NO)_6]^{2-}$ clusters possess structural cores different from that of $[Fe_4S_3(NO)_7]^{2-}$; on the other hand, the highest occupied molecular orbital of $[Fe_4S_3(NO)_7]^{2-}$ contains an unpaired electron, which has an antibonding character involving all pairs of iron atoms of the Fe_4S_3 core, leading

to an increase of the Fe−Fe bond lengths,[5c] while the $[Fe_6Se_6(NO)_6]^{2-}$ and $[Fe_6S_6(NO)_6]^{2-}$ clusters are similar to **3**, which are EPR-silent and have no unpaired electrons, as demonstrated by their perfect ^{1}H NMR spectra. This similar phenomenon has also been observed by Dahl and co-workers in the clusters $[Fe_4S_4(NO)_4]$ and $[Fe_4S_4(NO)_4]^{-}$.[6b]

The Fe−N bond distances for compound **1** range from 1.661 to 1.665 Å with an average of 1.663 Å. It is similar to the value of 1.667 Å in compound **2**, in which the Fe−N bond distances range from 1.659 to 1.672 Å. Accordingly, the N−O bond lengths in compound **1** range from 1.172 to 1.186 Å, with an average of 1.180 Å, which is also similar to the mean of 1.182 Å (from 1.168 to 1.197 Å) in compound **2**. When $[Fe_4S_3(NO)_7]^{2-}$[5c] and $[Fe_4S_3(NO)_7]^{-}$ (**3**) are compared, the Fe−N interactions are evidently strengthened in the dianion (average value: 1.646 vs 1.671 Å in the monoanion) owing to more back-donation from d_{Fe} to π^*_{NO}. On the other hand, the average N−O bond lengths are 1.176 Å for $[Fe_4S_3(NO)_7]^{2-}$[5c] and 1.166 Å for **3**, an opposite trend. These observations are consistent with the results of the IR spectra, which show that the absorptions of nitrosyl groups (ν_{NO}) appear at higher frequencies for complex **3**.

The Fe−N−O bond angles range from 174.5° to 178.9° with an average of 176.5°, which is close to linear. This indicates that the nitrosyl moieties exhibit sp-hybridized NO$^+$ character, which means that a considerable amount of charge transfer between NO and the metal took place.[20] The average Fe−N−O bond angle of 176.5° in complex **1** is similar to the average values of 174.4° in complex **2**, 176.9° in $[Fe_8S_6(NO)_8]^{2-}$,[11] 177.6° in $[Fe_4-S_4(NO)_4]$,[6b] and 177.5° in $[Fe_4S_4(NO)_4]^{-}$[6b] and the Fe−N−O bond angles of 177.6° and 178.3° arising from the apical Fe(NO) in $[Fe_4S_3(NO)_7]^{2-}$[5c] and complex **3**. However, it is clearly longer than the average Fe−N−O bond angles of 167.9° and 166.6° arising from the three sets of Fe(NO)$_2$ of $[Fe_4S_3(NO)_7]^{2-}$ and complex **3**, respectively. When comparing complex **3** with other Roussin's black salts, no differences could be attributed to the effects of the counterion besides the packing effects. These results show that the Fe−N−O bond angles of iron−sulfur (selenium) clusters are irrelevant to their dimension and charge but relevant to the number of nitrosyls attached to the iron atoms and the localized symmetry of the iron atoms.[6b,22] This also means that the variance[21b] of NO$^+$ (linear, sp-hybridized) and NO$^-$ (bent, sp^2-hybridized) may be brought out because of the greater deviations of the Fe−N−O bond angles from 180° in the iron dinitrosyl units for complex **3** and $[Fe_4S_3(NO)_7]^{2-}$.[5c]

Electrochemical Properties. The electrochemistry of complexes **1**−**3** was studied by CV, and the data are listed in Table 3. As shown in Figure 3, complex **1** shows two cathodic current peaks at $E_{pc} = -0.42$ and -1.36 V and three anodic peaks at $E_{pa} = -0.04$, -0.38, and -1.30 V; the peak at $E_{pc} = -0.42$ V is unusually strong with a full scan range from 0.40 to -1.80 V. In order to interpret the abnormal phenomenon, the CVs were scanned with different potential ranges. Interestingly, two quasi-reversible

(21) (a) Bourassa, J.; Lee, B.; Bernard, S.; Schoonover, J.; Ford, P. C. *Inorg. Chem.* **1999**, *38*, 2947–2952. (b) Jaworska, M.; Stasicka, Z. *J. Mol. Struct.* **2006**, *785*, 68–75.

(22) (a) Kettle, S. F. A. *Inorg. Chem.* **1965**, *4*, 1661–1663. (b) Enemark, J. H.; Feltham, R. D. *Coord. Chem. Rev.* **1974**, *13*, 339–406.

Table 2. Selected Bond Lengths (Å) and Bond Angles (deg) for **1**–**3** and the Reported $[Fe_4S_3(NO)_7]^{2-}$ [5c]

$[Fe_6Se_6(NO)_6]^{2-}$ (**1**)		$[Fe_6S_6(NO)_6]^{2-}$ (**2**)[7b]		$[Fe_4S_3(NO)_7]^{2-}$ [5c]		$[Fe_4S_3(NO)_7]^{-}$ (**3**)	
Fe1–Fe2	2.7254(8)	Fe1–Fe2	2.6402(11)	Fe1–Fe2	2.781(1)	Fe1–Fe4	2.6968(7)
Fe1–Fe3	2.7391(9)	Fe1–Fe3	2.6507(11)	Fe1–Fe3	2.757(1)	Fe2–Fe4	2.7104(7)
Fe2–Fe3	2.7267(9)	Fe2–Fe3	2.6399(12)	Fe1–Fe4	2.753(1)	Fe3–Fe4	2.7087(7)
Fe1–Se1	2.3364(7)	Fe1–S1	2.2211(15)	Fe2–S1	2.267(2)	Fe1–S1	2.2601(10)
Fe1–Se2	2.3425(8)	Fe1–S2	2.2238(15)	Fe2–S2	2.277(2)	Fe1–S2	2.2625(10)
Fe1–Se3	2.3445(7)	Fe1–S3	2.2154(16)	Fe3–S1	2.269(2)	Fe2–S2	2.2578(10)
Fe2–Se1	2.3473(7)	Fe2–S1	2.2130(15)	Fe3–S3	2.284(2)	Fe2–S3	2.2453(9)
Fe2–Se2	2.3430(7)	Fe2–S2	2.2292(16)	Fe4–S2	2.266(2)	Fe3–S1	2.2579(10)
Fe2–Se3	2.3362(7)	Fe2–S3	2.2174(16)	Fe4–S3	2.27 L(2)	Fe3–S3	2.2510(9)
Fe3–Se1	2.3431(8)	Fe3–S1	2.2216(16)	Fe1–S1	2.216(2)	Fe4–S1	2.2046(9)
Fe3–Se2	2.3290(7)	Fe3–S2	2.2136(15)	Fe1–S2	2.233(2)	Fe4–S2	2.2073(10)
Fe3–Se3	2.3487(7)	Fe3–S3	2.2282(16)	Fe1–S3	2.230(2)	Fe4–S3	2.2135(9)
Fe1–N1	1.665(4)	Fe1–N1	1.672(5)	Fe1–N1	1.653(7)	Fe1–N1	1.670(3)
Fe2–N2	1.661(4)	Fe2–N2	1.659(4)	Fe2–N21	1.665(7)	Fe1–N2	1.675(3)
Fe3–N3	1.663(4)	Fe3–N3	1.669(4)	Fe2–N22	1.644(7)	Fe2–N3	1.668(3)
N1–O1	1.172(4)	N1–O1	1.182(6)	Fe3–N31	1.618(7)	Fe2–N4	1.671(3)
N2–O2	1.186(4)	N2–O2	1.197(6)	Fe3–N32	1.662(7)	Fe3–N5	1.675(3)
N3–O3	1.183(4)	N3–O3	1.168(6)	Fe4–N41	1.652(7)	Fe3–N6	1.671(3)
Fe1–Se1–Fe3	71.66(2)	Fe1–S1–Fe2	73.08(5)	Fe4–N42	1.629(7)	Fe4–N7	1.670(3)
Fe1–Se1–Fe2	71.17(2)	Fe1–S1–Fe3	110.20(6)	N1–O1	1.172(6)	N1–O1	1.164(4)
Fe2–Se1–Fe3	110.05(3)	Fe2–S1–Fe3	73.05(5)	N21–O21	1.191(7)	N2–O2	1.167(4)
Fe1–Se2–Fe3	71.80(2)	Fe2–S2–Fe3	72.91(5)	N22–O22	1.176(7)	N3–O3	1.169(4)
Se2–Fe3–Se3	108.68(3)	S2–Fe3–S3	106.64(6)	N31–O31	1.181(8)	N4–O4	1.167(4)
Se1–Fe3–Se3	112.16(3)	S1–Fe3–S3	114.03(6)	N32–O32	1.169(7)	N5–O5	1.167(4)
Se2–Fe3–Se1	108.34(3)	S2–Fe3–S1	107.12(6)	N41–O41	1.165(7)	N6–O6	1.165(4)
Se1–Fe1–Se2	108.11(3)	S1–Fe1–S2	113.49(6)	N42–O42	1.181(7)	N7–O7	1.160(4)
Se2–Fe3–Fe1	54.33(2)	S2–Fe3–Fe1	53.50(4)	Fe1–N1–O1	177.6(6)	Fe1–N1–O1	170.4(3)
Se1–Fe1–Fe1	54.06(2)	S1–Fe1–Fe1	125.02(5)	Fe2–N21–O21	165.8(6)	Fe1–N2–O2	165.4(3)
Se3–Fe3–Fe1	124.52(3)	S3–Fe3–Fe1	53.16(4)	Fe2–N22–O22	170.4(7)	Fe2–N3–O3	167.1(3)
Se1–Fe2–Fe1	54.23(2)	S1–Fe2–Fe1	53.60(4)	Fe3–N31–O31	164.8(8)	Fe2–N4–O4	166.1(3)
Fe1–N1–O1	176.2(4)	Fe1–N1–O1	174.4(5)	Fe3–N32–O32	167.5(6)	Fe3–N5–O5	163.6(3)
Fe2–N2–O2	178.9(4)	Fe2–N2–O2	173.0(5)	Fe4–N41–O41	166.3(8)	Fe3–N5–O5	167.3(3)
Fe3–N3–O3	174.5(3)	Fe3–N3–O3	175.9(5)	Fe4–N42–O42	172.8(7)	Fe4–N7–O7	178.3(3)
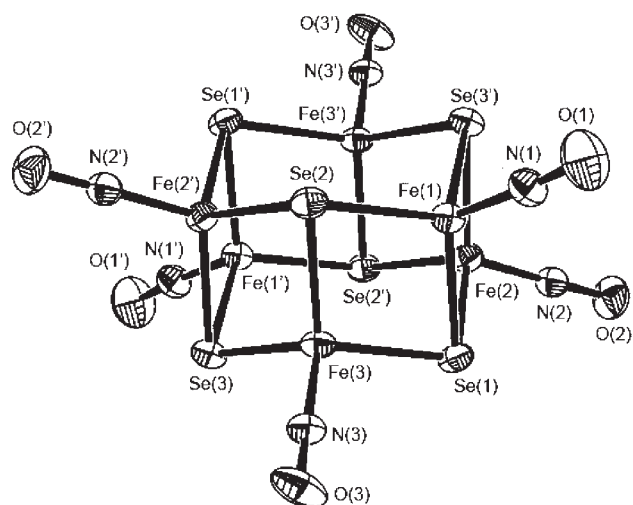
Figure 2. ORTEP diagram of compound **1** showing thermal ellipsoids with 50% probability. The counterion is omitted for clarity.

Table 3. List of Redox Potentials for Complexes **1**–**3** and the Reported Analogues

	redox potentials vs Fc^+/Fc (V)[a]				
		$E_{1/2}°$			
compound	E_{pa}				ref
$[(n\text{-}Bu)_4N]_2[Fe_6Se_6(NO)_6]$	–0.04	–0.41		–1.33	this work
$[(n\text{-}Bu)_4N]_2[Fe_6S_6(NO)_6]$	0.07	–0.33		–1.32	this work
$(PPN)_2[Fe_6S_6(NO)_6]$		–0.87		–1.70	8
$(Et_4N)_2[Fe_6S_6(NO)_6]$	–0.11[b]	–0.91	–1.08	–1.58 –1.82	4b
$(Me_4N)[Fe_4S_3(NO)_7]$		–1.09	–1.71	–2.21	this work
$(Et_4N)[Fe_4S_3(NO)_7]$		–0.86	–1.44	–1.93	4c
$(PPN)[Fe_4S_3(NO)_7]$		–0.54	–1.33		8

[a] In order to compare the literature data with our experimental data expediently, the reported redox potentials (vs SCE) in the references were converted to the values (vs ferrocene/ferrocenium[+]) in the table. [b] Reported $E_{1/2}°$ value.

reductions with half-wave potentials of −0.41 and −1.33 V with E_{pc}/E_{pa} separations of 60 and 70 mV were found when the range was set between −0.20 and −1.80 V. In addition, the cyclic voltammogram of the first reduction (E_{pc} = −0.42 V) and the two corresponding oxidation peaks (E_{pa} = −0.04 and −0.38 V) showed no change when the scan potential was set from +0.4 to −0.7 V, but the oxidation peak at −0.04 V was not observed when the potential was switched off at −0.10 V, showing that the oxidation peak at −0.04 V is the product of the reduction at −0.42 V. These results indicate that the intensity of the

unusually strong peak at E_{pc} = −0.42 V is a result of at least three processes. One is the quasi-reversible reduction at $E_{1/2}°$ = −0.41 V, and the other two are from an irreversible electrochemical process that occurred at E_{pc} = −0.42 V, in which the compound went through a typical electron transfer and chemical reaction (ECE) mechanism, of which its product is easier to reduce than the original one, resulting in an overlap of the reduction potentials and, subsequently, a very strong peak. The peak at E_{pa} = −0.04 V is the product from such a chemical reaction.

The redox behavior of compound **2** shown in Figure 4 exhibits two cathodic current peaks at E_{pc} = −0.30 and −1.29 V and three anodic peaks at E_{pa} = 0.08, −0.23, and −1.19 V when scanned from 0.40 to −1.80 V with a scan
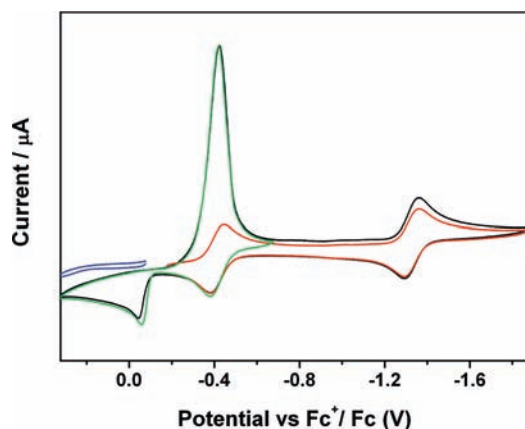
Figure 3. Cyclic voltammograms of a 1 mM solution of compound **1** in 0.1 M $(NBu_4)(PF_6)/CH_3CN$ at a scan rate of 0.1 V s^{-1}.
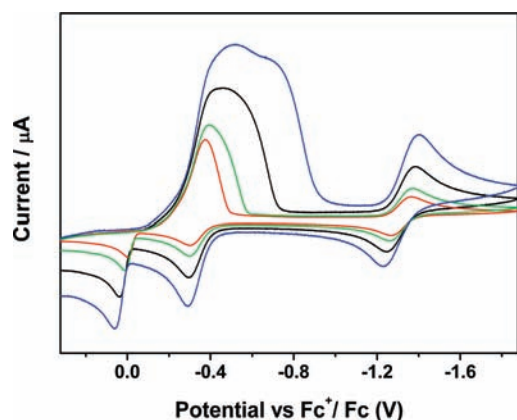

Figure 4. Cyclic voltammograms of a 1 mM solution of compound **2** in 0.1 M $(NBu_4)(PF_6)/CH_3CN$ at scan rates of 0.10 (red), 0.20 (green), 0.50 (black), and 1.00 (blue) V s^{-1}.

rate of 100 mV s^{-1}. It is similar to compound **1** in that the first reduction peak is much stronger than the second one. The cyclic voltammograms were also recorded using various scan rates from 0.1 to 1.0 V s^{-1}. As shown in Figure 4, when faster scan rates were applied, the first reduction peak was separated to two reductions. Meanwhile, the faster the scan rate, the clearer the separation observed between the two reduction peaks. However, the peaks that arose from the ECE process did not disappear even at a scan rate of 1 V s^{-1}, which indicates that the chemical step is quite fast. These observations are different from the reported cyclic voltammograms with the half-wave potentials of −0.87 and −1.70 V for $(PPN)_2[Fe_6S_6(NO)_6]$[11] and −0.11, −0.91, −1.08, −1.58, and −1.82 V for $(Et_4N)_2[Fe_6S_6(NO)_6]$.[7a] For the former, a possible reason is that a wider scan range (+0.40 to −1.80 V) was used in our

experiments than the one reported (0.0 to −1.80 V) in which one of redox courses could not be observed. For the latter, a reasonable explanation is that some factors, such as the counterion, electrolyte, electrode, and different starting scan potentials, caused two sets of one-electron reductions to overlap under our experimental conditions. Compound **3** bears three quasi-reversible reductions with half-wave potentials of −1.09, −1.71, and −2.21 V, which is similar to the values −0.86, −1.44, and −1.93 V reported for $(Et_4N)[Fe_4S_3(NO)_7]$ considering different counterion and test conditions.[5c]

Conclusions

In summary, iron−selenium and iron−sulfur nitrosyl clusters $[(n\text{-}Bu)_4N]_2[Fe_6Se_6(NO)_6]$ (**1**), $[(n\text{-}Bu)_4N]_2[Fe_6S_6(NO)_6]$ (**2**), and $(Me_4N)[Fe_4S_3(NO)_7]$ (**3**) have been synthesized by efficient solvent-thermal reactions, and their structures and properties have been studied by IR, UV−vis, ^{1}H NMR, electrochemistry, and single-crystal X-ray diffraction analysis. IR spectra of complexes **1** and **2** all display one strong characteristic NO stretching frequency (ν_{NO}) in solution with the characteristic of NO$^+$, while the IR spectrum of complex **3** displays three absorptions. The electronic absorption spectra show different bands in the range of 259−562 nm, which are assigned to the transitions between orbitals delocalized over the Fe−S cluster, the LMCT, π^*_{NO}−d_{Fe}, and the MLCT, d_{Fe}−π^*_{NO}. Single-crystal X-ray structural analysis reveals that complex **1** crystallizes in the monoclinic $P2(1)/n$ space group with two molecules per unit cell. Each iron center is bonded to three selenium atoms and a nitrogen atom from the nitrosyl ligand with a pseudotetrahedral center geometry. The two parallel "chair-shaped" structures, consisting of three iron and three selenium atoms, are connected by Fe−Se bonds. CV of compounds **1** and **2** display two cathodic and three anodic current peaks with an unusually strong cathodic peak. The experimental results indicate that the intensity of the unusually strong peak is a result of at least three processes. One is the quasi-reversible reduction, and the other two are from an irreversible electrochemical process, in which the compound went through a typical ECE mechanism. Compound **3** shows three quasi-reversible reductions.

Supporting Information Available: IR and ^{1}H NMR spectra of complexes **1**−**3** as well as the cyclic voltammogram and structural diagram of complex **3** and X-ray crystallographic files in CIF format for complexes **1** and **3**. This material is available free of charge via the Internet at http://pubs.acs.org.